# A model of Ponto-Geniculo-Occipital waves supports bidirectional control of cortical plasticity across sleep-stages

**Kaidi Shao**[1], **Juan F. Ramirez Villegas**[1,2], **Nikos K. Logothetis**[1,3,4], **Michel Besserve**[1,5*]

***For correspondence:**
michel.besserve@tuebingen.mpg.de

[1] Department of Physiology of Cognitive Processes, Max Planck Institute for Biological Cybernetics, Tübingen, Germany; [2]Institute of Science and Technology Austria (IST Austria), Am Campus 1, Klosterneuburg, Austria; [3]International Center for Primate Brain Research, Songjiang, Shanghai, China; [4]Centre for Imaging Sciences, Biomedical Imaging Institute, The University of Manchester, Manchester, UK; [5]Department of Empirical Inference, Max Planck Institute for Intelligent Systems and MPI-ETH center for Learning Systems, Tübingen, Germany

**Abstract** During sleep, cortical network connectivity likely undergoes both synaptic potentiation and depression through system consolidation and homeostatic processes. However, how these modifications are coordinated across sleep stages remains largely unknown. Candidate mechanisms are Ponto-Geniculo-Occipital (PGO) waves, propagating across several structures during Rapid Eye Movement (REM) sleep and the transitional stage from non-REM sleep to REM sleep (pre-REM), and exhibiting sleep stage-specific dynamic patterns. To understand their impact on cortical plasticity, we built an acetylcholine-modulated neural mass model of PGO wave propagation through pons, thalamus and cortex, reproducing a broad range of electrophysiological characteristics across sleep stages. Using a population model of Spike-Time-Dependent Plasticity, we show that recurrent cortical circuits in different transient regimes depending on the sleep stage with different impacts on plasticity. Specifically, this leads to the potentiation of cortico-cortical synapses during pre-REM, and to their depression during REM sleep. Overall, our results provide a new view on how transient sleep events and their associated sleep stage may implement a precise control of system-wide plastic changes.

**Significance statement:** Considerable evidence supports that sleep rescales cortical synaptic connections, requiring both long term potentiation to consolidate newly acquired memories, and long-term depression to maintain homeostatic levels of brain activity. However, which aspects of sleep activity contributes to this bidirectional control of plasticity remains unclear. This computational modelling study suggest that widespread transient phenomena called Ponto-geniculo-occipital (PGO) waves, have a sleep-stage dependent effect on plasticity. The alternation between sleep stages can thus be exploited in combination with spontaneously occurring transients, to trigger both up- and down-regulating effect on cortical connectivity, and may explain why the basic structure of sleep-cycles is a well-preserved property across mammalian species.

## Introduction

In most mammalian species, the brain undergoes drastic state changes between different sleep stages – Rapid-Eye-Movement (REM) and non-REM sleep – with broad behavioral and functional

similarities. There is moreover an emerging consensus on the existence of sleep-induced plastic changes in relation to two hypothesized functions: memory consolidation, and synaptic homeostasis (Buzsáky, 1998; Tononi and Cirelli, 2003, 2014). However, the detailed underlying mechanisms remain elusive and their investigation requires assessing the brain-wide impacts on plasticity of a variety of phenomena happening during sleep. So far, an extensive amount of experimental and computational modeling studies have focused on the neural bases of transient events observed in non-REM sleep (hippocampal ripples, cortical slow waves and thalamic spindles). In particular, it has been suggested that these non-REM events play a role in long term plastic changes necessary to memory consolidation (Steriade et al., 1993a; Sejnowski and Destexhe, 2000; Puentes-Mestril et al., 2019; Klinzing et al., 2019) and synaptic downscaling (Tononi and Cirelli, 2014, 2020; Watson et al., 2016). However, evidence suggests that key modifications of plasticity not only occur during non-REM but also during REM sleep (Grosmark et al., 2012; Datta and O'Malley, 2013; McDevitt et al., 2015; Boyce et al., 2016, 2017; Zhou et al., 2020).

Interestingly, the transitional stage from non-REM sleep to REM sleep (referred to as pre-REM stage), and the subsequent REM sleep stage are associated with the occurrence of another family of phasic events, Ponto-Geniculo-Occipital (PGO) waves (Steriade et al., 1989; Gott et al., 2017). A typical PGO wave displays biphasic waveforms in Local Field Potential (LFP) activity traces, comprising of a fast-negative component preceding a slower, weaker positive component, possibly followed by smaller fluctuations (Gott et al., 2017; Callaway et al., 1987; Datta, 1997). PGO waves are named after three key structures where their propagation is most frequently observed: the Pons, the Lateral Geniculate Body of the thalamus and the Occipital cortex (Jouvet, 1959). However they also manifest themselves in a broad range of brain structures and a variety of species, e.g. cats (Jouvet, 1959; Hobson, 1965; Datta, 1997), rodents (Kaufman and Morrison, 1981; Datta et al., 1998; Deboer et al., 1998, 1999), non-human primates (Cohen and Feldman, 1968; Ramirez-Villegas et al., 2020) and humans (Lim et al., 2007; Fernández-Mendoza et al., 2009). Importantly, during pre-REM and REM stages PGO waves exhibit two distinct subtypes (Bizzi, 1966): during pre-REM sleep they occur in high-amplitude singlets (Bowker, 1985), whereas REM PGO waves tend to cluster in 3-5 successive weaker deflections (Brooks, 1968; Bowker, 1985; Morrison and Pompeiano, 1966; Datta et al., 1992).

Given that converging evidence supports different roles played by non-REM and REM sleep stages in reorganizing networks across the brain (Grosmark et al., 2012; Seibt et al., 2017), the fact that PGO waves span both sleep stages in the form of two subtypes suggests that these events play a key role in coordinating plastic changes, and their analysis may provide insights into the differences between plasticity promoting mechanisms during non-REM and REM sleep. Indeed, experimental evidence supports a key role of REM-PGO waves in enhancing sleep-dependent learning and memory (Datta, 2000; Datta et al., 2003; Mavanji and Datta, 2003; Datta et al., 2004). In contrast, little is known about the impact of pre-REM PGO waves on plasticity. However, recent electrophysiological evidence for a coupling between sharp wave-ripples and PGO waves suggests PGO waves are involved in memory consolidation processes happening during non-REM sleep (Ramirez-Villegas et al., 2020).

While in-vivo investigations of PGO-triggered plasticity remains challenging, notably due to the spatial sparsity of the spines receiving PGO-associated potentials, and the expected weaker plastic changes induced by spontaneous activity, in contrast to those triggered by controlled sensory or electrical stimulation (Li et al., 2017; Yang et al., 2014; Zhou et al., 2020). As an alternative, investigating PGO waves from the computational modeling perspective may provide insights and guide further experimental studies. In particular, building a model of large-scale PGO waves propagation may help elucidate how the phasic potentials originated in the pontine region influences the widespread brain regions during sleep, and possibly controls their plasticity.

In this study, we use a multi-structure neural mass model to reproduce prominent features of PGO waves at a system level and shed light on their possible functions. By including cholinergic neuromodulation in our model, we put an emphasis on reproducing PGO-related phenomena

across sleep stages, and account for the variability of PGO wave subtypes occurring either during pre-REM or REM sleep. Finally, we investigate the putative influence on PGO waves on cortical plasticity through a mesoscopic model of spike time dependent plasticity, suggesting PGO waves have opposite effects in REM and pre-REM sleep. We provide insights on such state-dependent differences are achieved, suggesting a general framework to predict the influence of phasic events on plasticity.

## Results

### Ponto-geniculo-occiptial neural mass model

We designed a neural mass model to simulate average rate-coded population activities of several groups of homogeneous neurons (Wilson and Cowan, 1972, 1973; Jansen et al., 1993; Lopes da Silva et al., 1974) in three structures influenced by PGO waves: the pons, the thalamus (more precisely the lateral geniculate nucleus and the thalamic reticular nucleus) and the primary visual cortex.

Neural mass models represent the state of a population of identical neurons by the average firing rates across this population. The basic elements of such model are illustrated on Fig. 1A. The population average membrane potential evolves according to its intrinsic dynamics as well as post-synaptic currents it receives from connected populations, and outputs the population firing rate as a non-linear instantaneous function of the membrane potential using a sigmoidal activation. After multiplication with a synaptic strength coefficient, the output firing rate is convolved with the impulse response of the synapses that link the population to downstream neurons. Although neural mass models constitute a strong simplification with respect to single neuron models, recent work has shown they can reproduce sleep related phasic patterns, such as spindles and slow waves, with a satisfactory degree of realism, by taking into account key intrinsic currents flowing through the cells' membrane (Schellenberger Costa et al., 2016). We follow this approach to model PGO-wave propagation through pons, thalamus and cortex.

Specifically, our model involves 6 neuronal populations, as represented in Fig. 1B. The pontine population (R-PBL), representing low-frequency bursting PGO transferring neurons located in the rostral peribrachial area (R-PBL), receives high-frequency bursts from PGO triggering neurons located in the caudolateral peribrachial area (C-PBL) (Datta, 1997; Datta and Hobson, 1994; Datta, 1995; Datta and Hobson, 1995). The thalamus comprises 3 populations that are hypothesized to underlie PGO wave generation: the thalamocortical relay (TC) neurons in the lateral geniculate nucleus (LGN), the reticular thalamic (RT) neurons in the peri-geniculate nucleus (PGN) (Steriade and Llinás, 1988; McCormick, 1992) and the local intra-geniculate interneurons (LGin) in LGN (Hu et al., 1989a,b). In the cortex, following Schellenberger Costa et al. (2016), we model one excitatory population of pyramidal cells (Pyr), and one inhibitory interneuron population (In).

Considering the lack of clear experimental evidence elucidating what triggers the high-frequency bursts in the C-PBL PGO-triggering neurons (Datta, 1997), we model them as brief pulses — short-lasting rectangular signals (Fig. 1b) — in the population rate activity to reproduce the pooled bursting activities. Based on experimental traces of classical PGO waveforms and firing patterns of C-PBL neurons during both states (Datta and Hobson, 1994), pre-REM PGO waves are appropriately modeled with a single pulse while REM PGO waves are generated by several successive pulses (here we choose 3). The bursting interval (intervals between each two pulses) is fixed and selected from peri-PGO spiking histograms of C-PBL neurons (see also Fig. 1).

We incorporate specific key intrinsic currents in each population in order to model sleep oscillations related to memory consolidation processes, e.g. spindles, slow waves (see Table 1 for a summary and see Methods for details). In the pons, transferring neurons are equipped with a burst mechanism involving a cholinergic hyperpolarizing current (Leonard and Llinás, 1994). In the thalamus, TC and RT neurons both included a $K^+$ leaky current and a low-threshold Calcium T-current, together with a hyperpolarization-activated anomalous rectifier h-current in TC neurons (Destexhe et al., 1996; Schellenberger Costa et al., 2016). In the cortex, Pyr neurons possess a

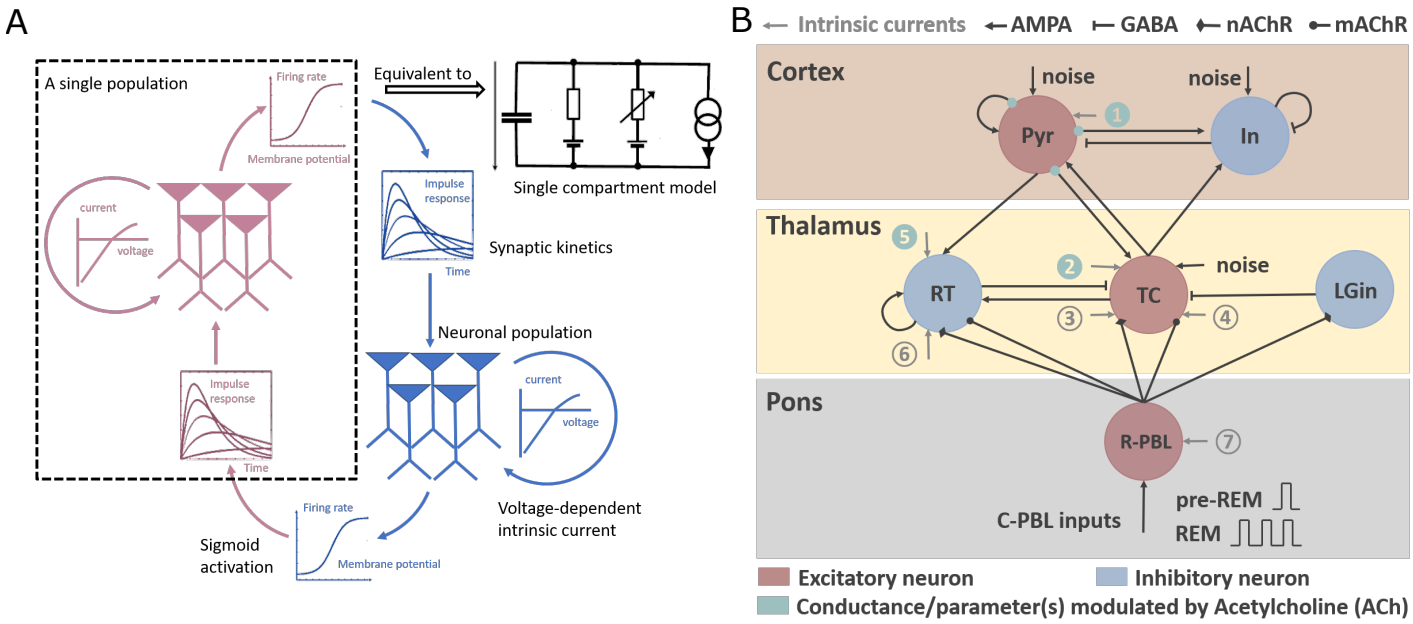


**Figure 1.** Neural mass model of PGO waves. (A) Illustration of the elements of neural mass models. Two neuronal populations modelled by neural masses are illustrated in separate colors. For a given population (marked in dashed rectangle) intrinsic and synaptic currents drive population membrane potential dynamics, which controls firing rate via a sigmoid activation curve. (B) Global view of the model structure, consisting of biologically plausible interconnected neuronal populations which receive brief pulses as inputs from C-PBL neurons to generate PGO-related neuronal activities. Switch of sleep stages are modulated by 4 major parameters (marked in green) associated with the change of Acetylcholine concentration. The circled numbers indicate intrinsic currents and are listed in Table 1, together with their role in state establishment or PGO wave generation. Abbreviation for neuronal populations: Pyr: Pyramidal neurons; In: inhibitory neurons; TC: thalamocortical neurons; RT: reticular thalamic neurons; LGin: interneurons in LGN; R-PBL: neurons in the rostal peribrachial nucleus (PGO-transferring neurons); C-PBL: neurons in the caudolateral peribrachial nucleus (PGO-triggering neurons). Abbreviation for receptors: AMPA: $\alpha$-amino-3-hydroxy-5-methyl-4-isoxazolepropionic acid; GABA: gamma-Aminobutyric acid; nAChR: nicotinic acetylcholine receptor; mAChR: muscarinic acetylcholine receptor.

| No. | Population | Intrinsic Currents | Role of intrinsic current |
|---|---|---|---|
| 1 | Pyr | $Na^+$-dependent $K^+$ current $I_{KNa}$ | Induction of K-complexes |
| 2 | TC | $K^+$ leaky current $I^t_{LK}$ | Modulation of membrane potential |
| 3 | TC | $Ca^{2+}$ T-current $I^t_T$ | Spindle generation |
| 4 | TC | Inward rectifier $K^+$ h-current | Wax and wining of spindle oscillation |
| 5 | RT | $K^+$ leaky current $I^r_{LK}$ | Modulation of membrane potential |
| 6 | RT | $Ca^{2+}$ T-current $I^r_T$ | Spindle generation |
| 7 | R-PBL | hyerpolarizating current | Generation of PGO-related bursts |

**Table 1.** List of intrinsic currents and their corresponding roles in each neuronal population

sodium-dependent potassium current $I_{KNa}$ to maintain the non-REM-related cortical oscillations (i.e. slow waves and K-complexes) (Sanchez-Vives and McCormick, 2000).

Neural mass models allow reproducing a wide range of electrophysiological characteristics to compare with the experimental findings. Apart from the population membrane potential and firing rates, we have access to the intrinsic and synaptic currents, enabling us to model the LFPs as a sum of transmembrane currents (Einevoll et al., 2013; Mazzoni et al., 2015) to characterize PGO waveforms. This provides a basis for comparing the outcome of our simulations to PGO waveforms reported in classical studies. Furthermore, following a mesoscopic approximation of the STDP rule (Fung and Robinson, 2013; Robinson, 2011), neural mass models will allow us to make theoretical predictions about the plastic changes at a given type of synapse.

## Establishment of non-REM and REM states

In order to model the two PGO wave subtypes appearing in pre-REM and REM sleep, the mechanisms underlying the experimentally observed electrophysiogical changes across sleep stages need to be incorporated in our model. Experimental evidence supports that the transition between non-REM and REM sleep is accompanied by the changing concentration of key neuromodulators, e.g. acetylcholine (ACh) and monoamines (Hobson, 2009; Diekelmann and Born, 2010). From non-REM to REM stages, concentration of the former rises when the latter recedes. Such anticorrelation thus allows us to model transitions between these states only by ACh-dependent influences. More specifically, ACh controls intrinsic conductances mediated by nicotinic/muscarinic acetylcholine receptors (nAChRs/mAChRs) (Hu et al., 1989a; McCormick and Prince, 1986; McCormick and Pape, 1988; McCormick and Bal, 1997). This includes the hyperpolarizing current of R-PBL neurons and potassium leaky currents in both thalamic neurons (see Methods section Cholinergic modulation of PGO waves for details). In cortex, cholinergic influence is modeled through ACh-dependent parameters modulating population excitability and the sodium-dependent potassium current (Disney et al., 2007; Soma et al., 2012). To match simulated activities to experimental findings, we use the maximum firing rate of the Pyr neurons as the ACh-related critical parameter and tune it to reproduce the peri-PGO firing rates and LFP waveforms of pre-REM and REM stages. Then ACh modulation of each parameter is imposed by a sigmoidal curve achieving a smooth transition between the low-ACh pre-REM value and the high-Ach REM value (see Fig. 2A).

Following this procedure, we first check whether the model reproduces long-term patterns of ponto-thalamo-cortical activity observed experimentally. Fig. 2B shows the LFPs in R-PBL, TC and Pyr neurons simulated in the whole network by tuning the ACh-modulated parameters shown in Fig. 2A, illustrating the contrast between the 3 scenarios: non-REM (pre-REM without PGOs), pre-REM (with PGOs) and REM sleep. During the simulated non-REM stage (Fig. 2B upper panel), R-PBL neurons do not burst, as shown in early studies (McCarley et al., 1978; Sakai and Jouvet, 1980; Steriade et al., 1990). TC neurons show strong spindle oscillations appearing with a frequency of occurrence of 0.1-0.2Hz in the simulated LFP. One can distinguish two spindle subtypes: type-I spindles are accompanied by slow waves in the Pyr neurons reflecting oscillations between two level of

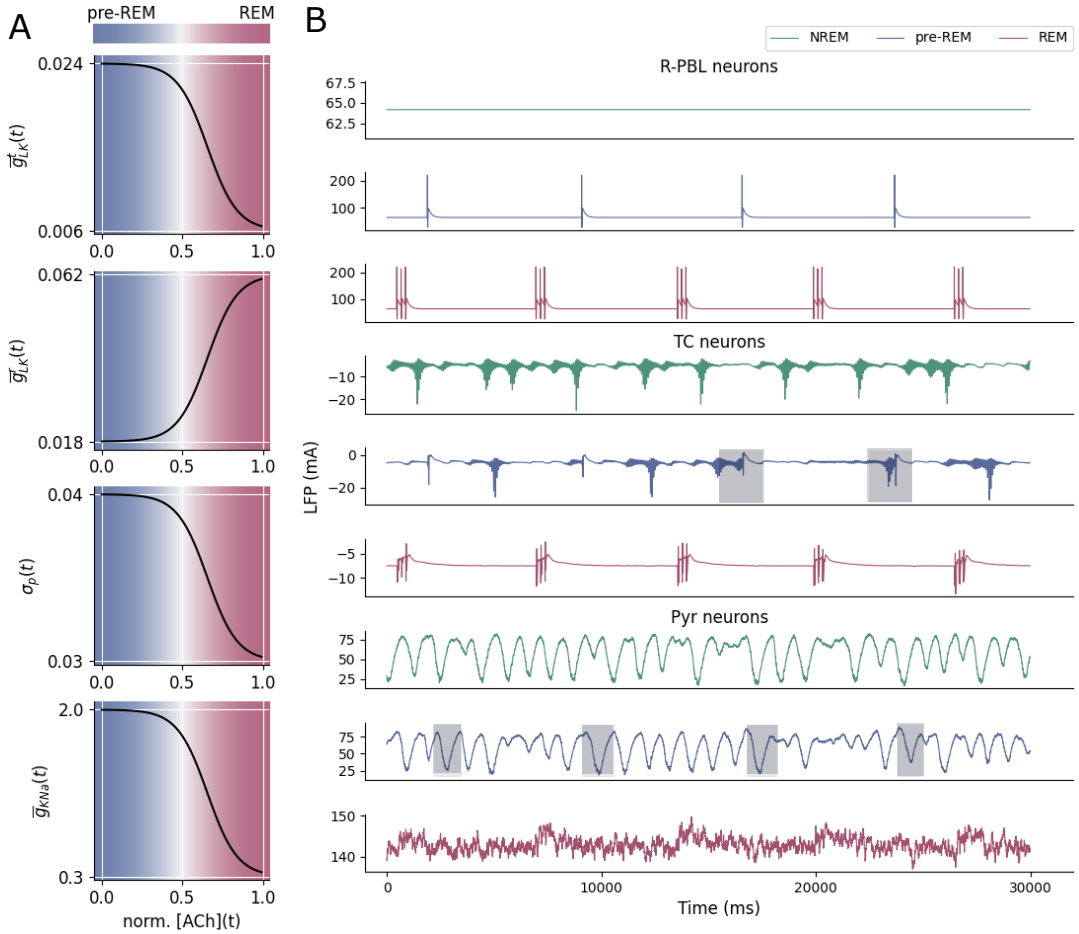


**Figure 2.** Establishment of sleep stages. (A) ACh-modulated model parameters. 4 critical parameters from the thalamocortical part are selected to reflect the cholinergic influence of the network. Their changes are linked to ACh concentration via a sigmoid-like relationship mimicking smooth stage switches. (B) State comparison of simulated LFPs in R-PBL (top), TC (middle) and Pyr neurons (bottom). LFPs of the three neuronal populations in three states (non-REM, pre-REM and REM) are plotted in separate colors for comparison. During pre-REM state, in the thalamus, contrary to non-REM state, spindles are interrupted by PGOs, as marked by grey shades in the trace of TC neurons during pre-REM stage. In the cortex, PGO waves trigger more slow oscillations during pre-REM, as marked by grey shades in the trace of Pyr neurons in pre-REM stage.

membrane potential: UP and DOWN states, while type-I spindles occur in isolation (without cortical slow wave) (Costa et al., 2016). In the presence of PGO inputs (Fig. 2B, top panel), biphasic patterns occur in R-PBL neurons triggered by PGO inputs. In the thalamus, some spindles are blocked by PGO inputs (Fig. 2B, middle panel, shaded areas), matching experimentally-recorded spindle interruption by phasic brainstem stimulations (Hu et al., 1989c). In cortex, pre-REM PGO waves trigger a succession of UP and DOWN states, thereby increasing the amount of slow oscillations with respect to non-REM stage (Fig. 2B, bottom panel, shaded areas). During REM stage (Fig. 2B, lower panel), thalamic spindles disappear with the depolarizing effect of the ACh-modulated current, as well as slow waves in the cortex. The activities of these simulated stages match the corresponding tonic electrophysiological traces shown in Steriade et al. (1989), supporting appropriate modeling of these states.

## Model Reproduction of Pontine and Thalamic neuronal activities

Beyond the sustained activities of pre-REM and REM states, we checked the ability of the model to replicate transient changes in PGO-triggered firing patterns reported by classical literature in cats (Steriade et al., 1989; Datta and Hobson, 1994; Steriade et al., 1990). Supplementary Fig. 1 show a comprehensive comparison between the key features of PGO-related neuronal activities in simulations and their experimental counterparts reported in classical electrophysiological studies in both pre-REM and REM stages. In the pons, the simulated peri-PGO histograms not only resemble the experimental ones in shape, but temporal characteristics also match quantitatively for bursting duration and onset latency, which are shown in detail in Supplementary Table 1. See Methods, section Pontine parameter tuning , for details on the tuning methodology.

In the thalamus, the similarities are reflected in the following aspects (Supplementary Fig. 1B). First, TC and RT neurons show differences in their baseline firing rates (indirectly membrane potentials), reflecting cholinergic modulation of thalamic membrane potentials via a potassium leaky conductance. TC neurons are more depolarized during REM than during pre-REM, while this is the opposite for RT neurons. As depolarization inactivates the T-curents of TC cells, state modulation also switches the dynamics of TC neurons from bursting during pre-REM, modeled by the sharp increase in firing rate at PGO wave onset, to non-bursting during the simulated REM state. In contrast, consistent with experimental studies (Steriade et al., 1989), RT bursting activity spans both sleep stages. Besides, on a finer scale, after bursting RT neurons undergo a slower hyperpolarization induced by the mAChR-receptor-mediated synapse, which is reproduced by the simulated events. Such hyperpolarization is also present during REM stage, contributing to the decreased response in RT neurons to the second and third pontine pulses. In line with experimental evidence, TC neurons show prolonged increased firing following their initial bursts (McCormick and Prince, 1987a; McCormick, 1992). Such sustained firing patterns are caused by activation of the cholinergic ponto-thalamic synapse mediated by a mAChR receptor, together with the dis-inhibition effect by RT neurons during their hyperpolarization (Hu et al., 1989b). In addition, the similarity between experimental and simulation results is significant (permutation test, $p<0.05$), as measured by a larger cosine similarity between PGO peri-event time windows in comparison with those from randomly selected trials as shown in Supplementary Fig. 1D These similarities all validate the reliability of the model in replicating cellular in-vivo activity, supporting it can serve as a steppingstone to investigate plasticity induced by PGO wave activities.

## Model Reproduction of thalamocortical LFP

We further checked the model is also able to reproduce the typical PGO-triggered LFP waveforms in the thalamus and cortex, which were more frequently recorded in early reports of PGO waves. A comparison of the LFP waveforms and corresponding spectrograms between two subtypes of PGO waves is shown in In Fig. 3A-B. The simulated thalamic activity can capture many features of the experimental waveforms (compared to traces in e.g. Callaway et al. (1987)), such as the biphasic pattern consisting of the negative and positive deflections, as well as the stronger amplitude

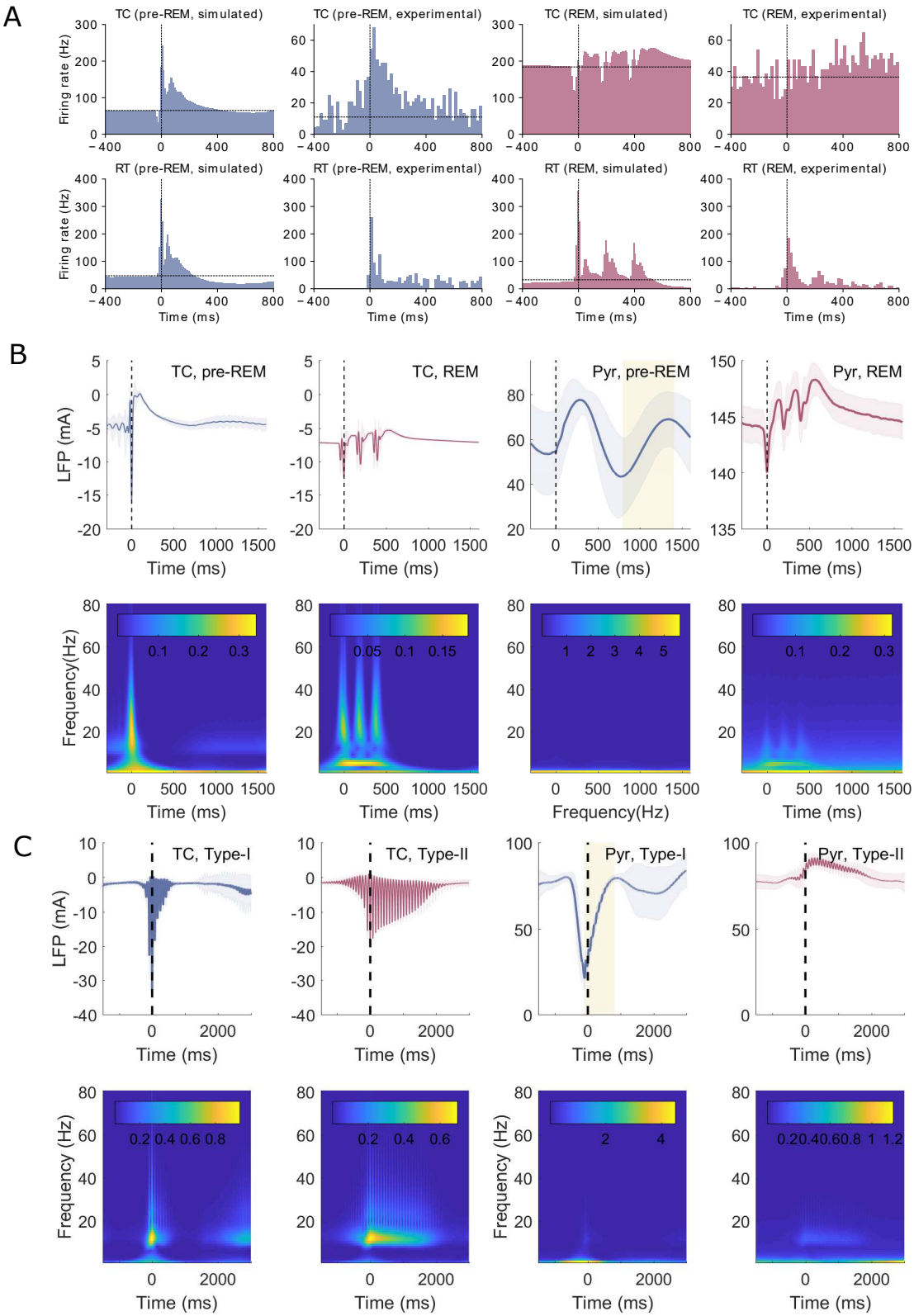


**Figure 3.** Model Reproduction of thalamocortical LFP. (A) Averaged events and normalized peri-event spectrogram of TC and Pyr neurons during pre-REM and REM PGO waves. Half-transparent shades represent the standard deviation of time-varying events across 1000 trials. Yellow shades mark the DOWN→UP state transition in the cortex. (B) Same as A for type-I and type-II spindles. (C) Comparison of normalized power spectrum for all the conditions. Power spectrum are computed by an average across time and normalized by frequency-wise standard deviation. Shades reflect variability across 1000 trials (trial-wise standard deviation).

of the negative peak of the pre-REM subtype. Moreover, the duration of the simulated waveforms (approximately 500ms) matches the experimentally recorded waveforms (e.g. in Callaway et al. (1987); Steriade et al. (1989); Nelson et al. (1983)). Spectrograms of the two subtypes in both thalamus and cortex also show that the pre-REM PGO waves are prominent in lower frequency bands compared to REM PGO waves. The reproduction of these electrophysiological characteristics may depend on the parameter tuning of the five ponto-thalamic projections cooperatively transforming the pulse-like pontine outputs into the subtypes' specific waveforms in the thalamus. We investigated whether all of these projections play a role in the waveform shapes by comparing our result to simulations resulting from suppressing one projection at a time (see Methods, section Validation of Ponto-thalamic projections). Overall, this analysis supports that taking into account all ponto-thalamic projections is necessary to replicate the REM-PGO waveforms (see Supplementary Fig. 2).

We additionally investigated the differences between the PGO waveforms and another key sleep event, observable in thalamus and cortex during NREM sleep, the spindles. Comparing spectrograms and the averaged spectra (Fig. 3B-C), spindles in the thalamus oscillate in a higher frequency band than both PGO waves. Moreover, while Type-I spindles and pre-REM PGO waves are both associated to DOWN-to-UP state transition in the Pyr neurons of the cortex, spindles occur after an UP-to-DOWN transition is initiated by cortex, while pre-REM PGO waves first initiate an UP-state followed by a slow oscillation between DOWN and UP states. This observation, as well as the time scale (200-300ms), matches well with experimental recordings showing that stimulation of the cortex triggers DOWN→UP transitions (Levenstein et al., 2019).

## PGO-triggered cortical plasticity, compared to spindle-triggered plasticity

After this comprehensive validation of the model's ability to reproduce many electrophysiological aspects, we use the simulated PGO-triggered activities to explore what plasticity effects PGO waves could induce in the cortical pyramidal neurons. Following a plasticity framework for mean-field models proposed by Robinson (2011) and Fung and Robinson (2013), we introduce a time-dependent plasticity rule for neural mass models. The change of synaptic strength $N_{mk}$ between an afferent population $m$ and an efferent population $k$ depends on the simultaneous change of synaptic current $J_m^k$ and postsynaptic firing rate $Q_k$:

$$\frac{dN_{mk}}{dt} = \int_{-\infty}^{+\infty} \left\langle Q_k(t+\tau) H(\tau) J_m^k(t) \right\rangle_t d\tau = \int_{-\infty}^{+\infty} \left\langle Q_k(t+\tau) J_m^k(t) \right\rangle_t \cdot H(\tau) d\tau \tag{1}$$

where $H(\tau)$ is the STDP function shown in Fig. 4B and the bracket denotes a time averaging. The STDP function's parameters are taken from in vitro measurements in hippocampal cell cultures (Bi and Poo, 1998).

Simply put, this equation shows that the sign and strength of plastic changes are determined by the similarity between the classical STDP window (Fig. 4B) and the cross-correlation between the pre- and post-synaptic activities, measured by the intergral of their product of over time. In the context of our model, we are interested in the plasticity of cortico-cortical excitatory connections, in which the presynaptic current is the excitatory AMPA current that the Pyr population sends to itself, and the postsynaptic firing rate measures the postsynaptic activities (Fig. 4A). By applying the STDP rule to the PGO-triggered cortical AMPA current and the firing rate of Pyr neurons, we find that the synaptic change is different when they are triggered by different PGO wave subtypes. The strength of intra-cortical excitatory synapses rises sharply during pre-REM PGO waves while increases slowly during no-PGO periods, suggesting that pre-REM PGO waves are important contributors of LTP during this sleep-stage (Fig. 4C, left panel). In contrast, REM-PGO waves elicit Long-term Depression (LTD) in the same synapses (Fig. 4C, right panel).

To interpret the differentiated plastic effects induced by the two PGO subtypes, the cross-correlation between the pre- and post-synaptic activities exploited by the STDP rule implementation is shown in Fig. 4D. As the presynaptic AMPA current in the Pyr module is the postsynaptic firing rate convolved with an alpha function, according to system theories there should always be

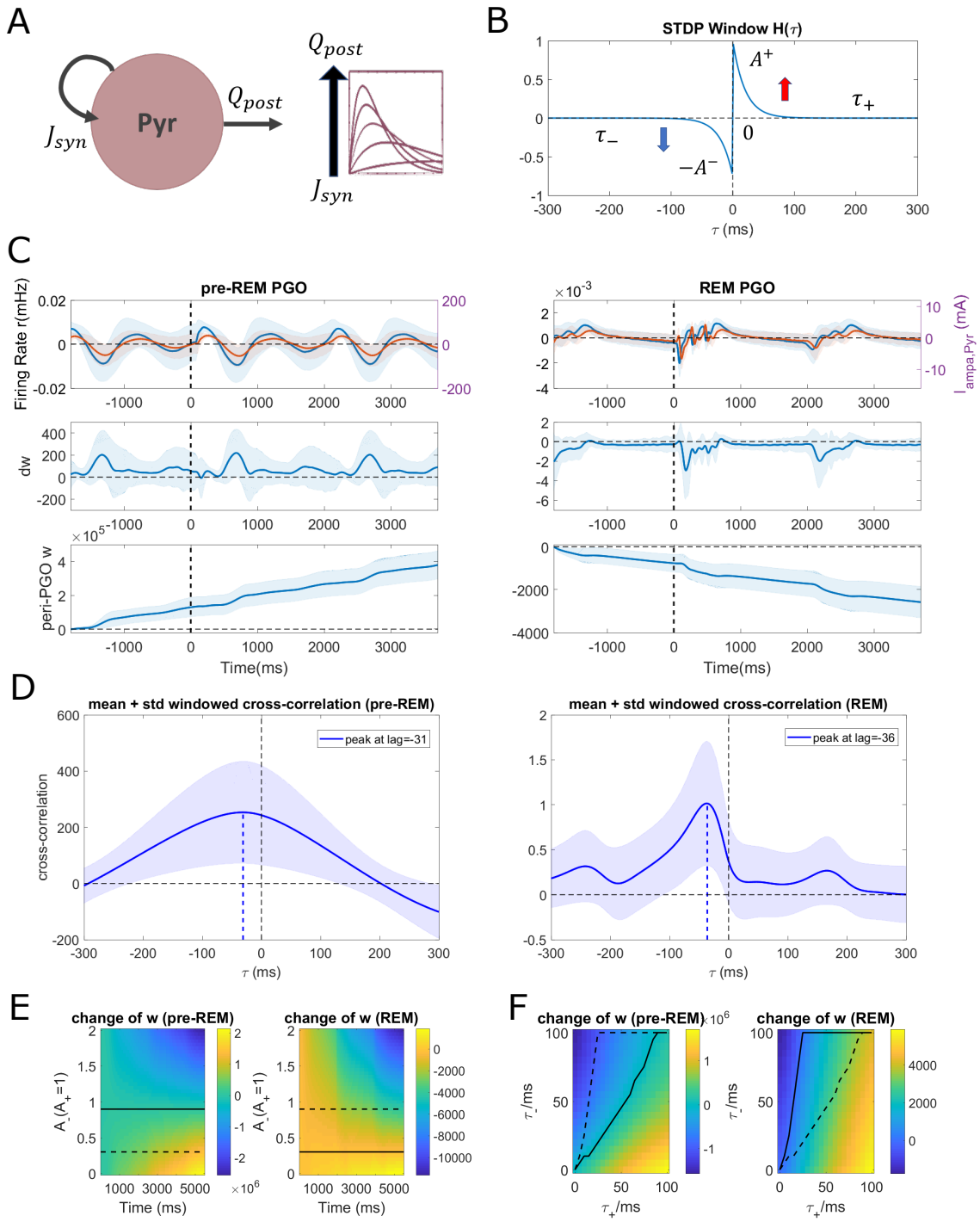


**Figure 4.** PGO-triggered cortical plasticity. (A) Illustration of the relationship between pre-synaptic current and post-synaptic firing rate in the cortical model. (left) Intra-cortical plasticity is studied at the excitatory AMPA-receptor-modulated synapse from the Pyr neuronal population to itself. (right) The current can be understood as the firing rate convolved with a linear system whose impulse response characterized by an alpha function. (B) Illustration of the STDP window. The horizontal axis $\tau$ represents the time difference between pre- and post-synaptic activities. The Positive peak on the right half plane suggests that the synapse gets strengthened when pre-synaptic actvities elicit post-synaptic ones, and vice versa for the opposite sequence. (C) Smoothed change of synaptic strength in the intra-cortical excitatory synapse evoked by two subtypes of PGO waves. (top) demeaned waveforms of pre-synaptic current (red) and postsynaptic firing rate (blue). (middle) time-varying change of synaptic strength. (bottom) synaptic strength of the intra-cortical excitatory synapse changing with time. (D) Comparison of cross-correlation between the pre-synaptic current and the post synaptic activities. Grey shade represents standard deviation at each lag for all the trials calculated. (E) Effect of STDP parameter $A^-$ on the plasticity direction induced by two PGO subtypes. Color bar indicates the relative increase/decrease of synaptic strength across time. Solid lines marks the critical value of the parameter that switches plasticity direction, i.e. potentiation v.s.de-potentiation; dashed lines correspond to the critical values of other subtype. (F) Effect of STDP parameters $\tau_+$ and $\tau_-$ on the plasticity direction induced by two PGO subtypes. Color bars and lines are analogous to E.

a lag in the cross-correlation, regardless of the subtypes, as reflected by the similar location of the maximum cross-correlation lag in both cases (Fig. 4D). However, another characteristic of the cross-correlation differs between the pre-REM and REM PGO events: the cross-correlation in pre-REM is much flatter than during REM, explaining the sign difference of plasticity. Indeed, for pre-REM cross-correlations, the flat autocorrelation implies that equation 1 while be approximately proportional to the integral of the STDP window of Fig. 4B. Because this function has a larger positive area (in the positive lags) than the negative, this leads to an overall positive synaptic change. For the REM case, the asymmetry of the cross-correlation puts more weight in the negative lag portion of the integral of eq. 1, resulting in negative portion of the STDP function overweighing the positive region, leading to an overall negative change of synaptic strength.

The STDP rule we adopt, like most other commonly-used ones, is sensitive to the selection of parameters of the STDP window: the positive amplitude $A^+$, the negative amplitude $A^-$, the time constants $\tau_+$ and $\tau_-$. The sign and relative magnitude of plastic changes being unchanged by an overall rescaling of the STDP function, we fix the positive amplitude to a constant $A^+ = 1$ for this analysis. Fig. 4E-F show how the switch of LTP/LTD induction is modulated by changing these parameters. The region comprised between the solid and dashed line shows the domain of STDP function parameters ensuring pre-REM PGO waves are accompanied with an increase of synaptic strength while REM PGO waves occur with a decrease of synaptic strength. As demonstrated by our above results, the biologically-measured STDP window parameters measured by classical studies (Bi and Poo, 1998) falls into this region ($A^+ = 1$; $A^- = 0.75$, $\tau^+ = \tau^- = 20ms$).

In order to interpret the dynamics of other memory-relevant sleep events from a cortical plasticity perspective, we also applied the same STDP framework to the two subtypes of spindles simulated during non-REM stage (Supplementary Fig. 3). Type-I spindles induce LTP-like behavior in the cortico-cortical connections, which makes sense as the peri-spindle neurons' activities exhibit a similar pattern as pre-REM PGO waves. Interestingly, type-II spindles lead to a much weaker (see axis scale) temporal increase of the synaptic strength before it returns to a lower level. This analysis supports that type-II spindles induce a weaker LTP than type-I. This is in agreement with experimental calcium imaging data indicating that the co-occurrence of spindles and slow oscillations, corresponding to type-I spindles, leads to stronger increases of dentritic calcimum in cortical neurons, which in turn are prone to trigger large plastic changes, compared to isolated (type II) spindles (Niethard et al., 2018). Overall, our analysis suggests that spontaneous sleep events occurring in the cortico-thalamic system are potentiating the cortico-cortical connections during non-REM sleep (including pre-REN) and depressing during REM sleep, implying a complementary role for these stages.

## Discussion

In this study, we have shown that an acetylcholine-modulated ponto-thalamo-cortical neural mass model spanning three sleep stages, non-REM, pre-REM and REM, can reproduce a series of electrophysiological features associated with PGO waves, including the differences in firing rate patterns and LFP waveforms of two PGO wave subtypes. Analysis of cortico-cortical plasticity associated to these events, as well as spindles, suggests a sleep-stage dependent role: non-REM and pre-REM sleep events inducing long-term potentiation, while REM events lead to long-term depression.

The choice of a neural mass model helps to maintain the realism of the model by trading off the complexity that would have incurred using individual units. It possesses the ability to account for detailed properties of synaptic and intrinsic currents based on quantitative experimental results, in particular the acetylcholine-modulated state-switching conductance and the five ponto-thalamic cholinergic projections, as the key of the generation of PGO-triggered neural activities. It is worth noting that among these projections, the results support the importance of including a population of local geniculate interneurons receiving pontine input, which is often neglected in previous thalamocortical models (Muller and Destexhe, 2012). This is to the best of our knowledge the first computational model accounting for the detailed cellular mechanisms of thalamic PGO wave

generation, clarifying details in the classical electrophysiological literature (Hu et al., 1989a; Datta, 1997) as well as paving the way for future single unit models of PGO waves.

The STDP framework for neural field theory, which has proved effective in characterizing TMS-induced plasticity (Wilson et al., 2014, 2018), is extended here to neural mass models deprived from spatial structure. The STDP rule, computed with parameters estimated experimentally in-vivo (Bi and Poo, 1998), reveals an opposite plasticity effect of two subtypes of PGO waves – potentiation for pre-REM PGO waves and depression for REM PGO waves.

These results support the ability of PGO waves to up- and down-scale cortical synaptic weights in larger proportions than the baseline activity surrounding them, making them candidates to enforce synaptic homeostasis, a role that spontaneous phasic sleep events are hypothesized to play in line with considerable experimental evidence (Niethard et al., 2018; Gridchyn et al., 2020). Our results for REM PGO waves, for which the contribution to synaptic homeostasis remained elusive, is in line with the downscaling effect of REM sleep on cortical spike rates observed in rats in Watson et al. (2016), and possibly matches the eliminated spines during REM sleep in mouse reported by Zhou et al. (2020). In contrast, the potentiation effects that we found for pre-REM PGO waves, although apparently contradictory to the classically attributed depotentiating role of non-REM sleep, is still consistent with results in Watson et al. (2016), as such downscaling maybe affect only a specific subgroup of synapses, with the largest synaptic weights in the population, while other subgroups may undergo potentiation to ensure consolidation of newly acquired memories (as predicted in Levenstein et al. (2017)). Indeed, converging evidence suggest that interacting non-REM events may be involved in consolidating specific memory traces into local neural microcircuits, with the slow-wave-ripple coupling a specific example (Maingret et al., 2016; Latchoumane et al., 2017; Klinzing et al., 2019). Interestingly, as reported by Ramirez-Villegas et al. (2020), pre-REM PGO waves co-occur with sharp-wave ripples, while our results exhibit a co-occurrence of pre-REM PGO waves and slow waves (specifically DOWN→UP state transitions). According to synaptic plastic pressure theory proposed by Levenstein et al. (2017), ripples, associated with off-line reactivation of episodic memories, occurring during DOWN→UP state transitions provide an opportune time window for new memory traces with low average firing rates to get assimilated into the existing network with relatively high firing rates. Pre-REM PGO waves may serve as trigger and facilitator of this procedure.

Overall, our results suggest the variability of neuronal patterns observed during sleep, may serve the purpose of differentially affecting the plasticity of network elements. The multiphasic nature of these events and their grouping in time, may put the network in a dynamical state that ensures the right synapses can be targeted for plastic changes despite the strong recurrence of the microcircuit they are embedded in. The idea that specific events are optimal to trigger certain plasticity mechanisms resonates with recent experimental results showing spindles result in a targeted increase of calcium activity in cortical dendrites during non-REM sleep, suggesting that these events are able to trigger dendritic depolarization independent of somatic activity (Seibt et al., 2017). Our results suggest further experimental work should be conducted on the characterization of transient REM activity, and parallel with a detailed modeling of the optimality of transient events for triggering synaptic plasticity processes in recurrent microcircuits.

## Methods

### Origin of model choice

Our model focus primarily on the reproduction of electrophysiological characteristics of PGO waves in the thalamus, where experimental PGO WAVE traces are most prominent and cellular mechanisms are relatively clear after extensive investigations in the field. Well-replicated thalamic PGO waves enable us to speculate on the effect PGO wave triggers in the cortex. Therefore, it is natural that we take as a starting point a neural mass model of thalamocortical network proposed in Schellenberger Costa et al. (2016), whose cortex and thalamus module, as well as the thalamic neuronal

types (the TC and RT neurons), match well with our purpose. What we need to do, is to add the LGin neurons and connect it with the pons in a biologically-realistic way.

This model is able to reproduce signatures of non-REM sleep, e.g. thalamic spindles and K-complexes in the cortex, by incorporating various intrinsic currents to generates specific neuronal activities (e.g. bursting). Thus, elaborating the model would also facilitate the investigation of interactions between PGO waves with these non-REM events.

To model the intrinsic properties of thalamic neurons, we follow the literature exploited in this thalamocortical model (Destexhe et al., 1996; Schellenberger Costa et al., 2016), i.e. a $K^+$ leaky current and a low-threshold Calcium T-current in both neurons populations, together with a hyperpolarization-activated anomalous rectifier h-current in TC neurons.

The cortex is simplified as a population of pyramidal cells interacting with a group of inhibitory neurons. Similarly, for the cortex, we keep the intrinsic current - a sodium-dependent potassium current $I_{KNa}$- in Pyr neurons so as to maintain the non-REM-related cortical oscillations (i.e. slow waves and K-complexes).

Following a major hypothesis of thalamic PGO wave generation Hu et al. (1989a), we added another population representing LGin neurons using the same framework. As for LGin neurons, we don't make any assumptions in its intrinsic currents or its role in spindle generation due to limited knowledge (Zhu et al., 1999).

## Differences between our PGO model and the original thalamocortical model

The structure of our model is identical to the original model, including neuronal types, synaptic connections and intrinsic currents, except the inclusion of LGin neurons in the cortex which does not interfere with the thalamocortical interactions. Most model parameter are picked from the parameter settings in the N3 state of the original model from their C++ implementations), except for a few changes:

1. Critically, for the modeling of neuromodulatory effects (see below), we set different values to the maximum conductance for the leaky potassium channels in TC and RT, which used to be the same in the original model.
2. to avoid additional spindle-like oscillations induced by the PGO waves (see Results), we weakened the connection from Pyr neurons to RT neurons, and balanced their potassium leaky conductance accordingly to restore the N2 state for spindle generation and N3 state as the pre-REM state.
3. we adjusted the noise levels in both the thalamus and the cortex to maintain a preferred frequency of spindle occurence.

## Modeling methodology

### Neural mass models

Neural mass models reflect average rate-coded population activities of a group of homogeneous neurons (Jansen et al., 1993; Lopes da Silva et al., 1974), where the mechanisms are briefly discussed in Results and illustrated in Fig. 1. Although neural mass models constitute a strong simplification with respect to single neuron models, recent work has shown such model can reproduce sleep related phasic patterns with a satisfactory degree of realism by taking into account intrinsic currents flowing through the cells' membrane (Schellenberger Costa et al., 2016).

### Firing rates

The firing of a given population of neurons is assumed to be elicited when its average membrane potential goes beyond a threshold. Thus in a simplified implementation the firing rate $Q_k$ of a neuron population $k$ is activated through a sigmoidal function of its instantaneous membrane potential $V_k$ :

$$Q_k = \frac{Q_k^{max}}{1 + \exp(-(V_k - \theta_k)/\sigma_k)} \tag{2}$$

In this function, $\theta_k$ denotes the physiological activation threshold which can be obtained from experiments; $\sigma_k$ is the activation gain that is often influenced by neuromodulators and more generally the brain state.

### Intrinsic currents

Both intrinsic currents and synaptic currents affect the cells' membrane potentials. Modelling intrinsic currents amounts to modeling the membrane's ion channels because they are only driven by the membrane itself instead of being activated by presynaptic neurons. The current that passes through a channel $i$ in population $k$ is classically expressed as the product of a fixed maximum conductance $\overline{g}_i$ (representing the conductance when the channel is completely open) with a potential difference between the membrane potential $V_k$ and the reversal potential $E_i$ of the channel (as a driving force). Depending on the electrophysiological characteristics of a channel, sometimes an additional factor is used to model a voltage- (or ion-concentration-) dependent opening probability of the channel. As a consequence, an voltage-dependent intrinsic current from channel $i$ in a population $k$ is modeled in the form:

$$I_i^k = \overline{g}_i \cdot g(V_k) \cdot (V_k - E_i) \tag{3}$$

An important intrinsic current that controls the resting membrane potentials of TC and RT neurons is the $K^+$ leaky current (Krishnan et al., 2016). The voltage-independence of its opening probability is implied by its name, as 'leaky' refers to the channels with a linear I-V curve. Thus in population $k$ this leaky current (with reversal potential $E_k$ for $K^+$) is denoted $I_{LK}^k$ and modeled as:

$$I_{LK}^k = \overline{g}_{LK}^k \cdot (V_k - E_K) \tag{4}$$

In addition, both TC and RT neurons possess a low-threshold Calcium T-current that generates rebound bursts in their firing patterns. The bursts are generated because de-inactivation threshold of a T-current is lower than the resting membrane potential - it can only be de-inactivated upon hyperpolarization, so that bursting activities are caused by the overlapping time regime between the voltage-dependent gating of activation and inactivation. The modeling of T-currents in population $k$ follows a Hodgkin-Huxley formulation, i.e. the opening probability is written in the form of products of two voltage-dependent gating variables $m_\infty^k$ and $h_T^k$ representing respectively the activation and inactivation variables of this Calcium channel (see Destexhe et al. (1998) for more details).

$$I_T^k = \overline{g}_T^k \cdot \left(m_\infty^k\right)^2 \cdot h_T^k \cdot (V_k - E_{Ca}) \tag{5}$$

The T-currents in the two neuron types show distinct characteristics in bursting frequency and acceleration. The underlying cellular differences involve (in)activation potentials and time constants of the gating variables, which were already investigated and quantified in earlier studies (Destexhe et al., 1994, 1996, 1998).

The h-current in TC neurons, controlling the waxing and waning of spindles is also called an anomalous inward rectifier because its conductance decreases with the rising of membrane (Steriade and Llinás, 1988). Following what was implemented in the original model, we assume that the opening probability change is due to extracellular $Ca^{2+}$ concentration, whereas the time constants were fitted using experimental results (Destexhe et al., 1996):

$$I_h^k = \overline{g}_h \cdot (m_{h1}([Ca^{2+}]_o) + g_{inc} \cdot m_{h2}([Ca^{2+}]_o)) \cdot (V_k - E_h) \tag{6}$$

In the cortex, the generation of slow waves and K-complexes is mediated by a sodium-dependent potassium current in Pyr neurons, where the conductance depends on sodium concentration $[Na]$:

$$I_{KNa} = g_{KNa} \frac{0.37}{1 + (\frac{38.7}{[Na]})^{3.5}} \cdot (V_k - E_h) \tag{7}$$

$$[\dot{Na}] = (\alpha_{Na} Q_e(V_e)) - Na_{pump}([Na])/\tau_{Na} \tag{8}$$

## Postsynaptic currents

Apart from intrinsic currents, the action potentials of afferent populations of neurons also affect the membrane potential dynamics through a variety of chemical synapses. In the typical case of chemical synapse, neurotransmitters released due to the activation of the presynaptic neuron diffuse in the synaptic cleft and lead to the opening of targeted ion channels on the postsynaptic membranes.

Here we assume a monosynaptic connection $m$ from presynaptic neuron population $k'$ to postsynaptic population $k$. Then a synaptic current $J_m^k$ obeys

$$J_m^k = P_m \cdot (V_k - E_m) \tag{9}$$

where $P_m$ is the opening probability of postsynaptic channels. Unlike intrinsic currents, $P_m$ is not only dependent of the target population's own membrane potentials $g(V_k)$, but also on the instantaneous concentration of released neurotransmitters, i.e.

$$P_m = s_{mk} \cdot g(V_k) \tag{10}$$

where $s_{mk}$ represents the opening probability caused by neurotransmitters.

$$s_{mk}(t) = N_{k'k} \cdot Q_{k'}(V_{k'}(t)) \otimes h_m(t) \tag{11}$$

Therefore the complete model for the synapse can be written as

$$J_m^k(s_{mk}) = s_{mk} \cdot g(V_k) \cdot (V_k - E_m) = N_{k'k} \cdot Q_{k'}(V_{k'}(t)) \otimes h_m(t) \cdot g(V_k) \cdot (V_k - E_m) \tag{12}$$

Compared to the general form of intrinsic currents, the product of the synaptic strength and maximum firing rate of presynaptic neuron $N_{k'k} \cdot Q_{k'}^{max}$ can be seen as equivalent to the maximum conductance (Eq. 2). It is general be free to adjust $N_{k'k}$ as it depends on many biological parameters of the network for which we do not have a reliable estimate (synaptic strenghts, number of synapses per cell, etc.). The impulse response $h_m$ can be approximated using the time course of postsynaptic currents (PSCs) in response to brief pulses that can be obtained in voltage-clamp experiments. A common approach to approximate such impulse responses is to model them as an alpha function:

$$h_m = \gamma_m^2 \cdot t \exp(-\gamma_m t) \tag{13}$$

The alpha function reaches its peak value at the time point $\gamma_m^{-1}$. Such impulse response corresponds to a second order linear dynamical system. As a consequence, the opening probability can be written in the form of a differential equation (for derivation, see Appendix. A):

$$\ddot{s}_{mk} = \gamma_m^2 \cdot (N_{k'k} \cdot Q_{k'}(V_{k'}) - s_{mk}) - 2\gamma_m \cdot \dot{s}_{mk} \tag{14}$$

which is thus easy to simulate using classical iterative methods.

Most experiments revealing the PSC of an ion channel characterize its kinetics with a rise time and a decay time, which is imcompatiable with the alpha function. To incorporate these temporal features, an alternative impulse response could be a concatenation of two first-order linear systems with different time constants (referred later as 'two-exponential'). In the time domain, it take the following form:

$$h_m = B \cdot (\exp(-t/\tau_1) - \exp(-t/\tau_2)) \tag{15}$$

where $B$ is the normalization term:

$$B = ((\frac{\tau_2}{\tau_1})^{\tau_{rise}/\tau_1} - (\frac{\tau_2}{\tau_1})^{\tau_{rise}/\tau_2})^{-1} \tag{16}$$

In this formula, $\tau_{rise}$ denotes the rise time, whereas the decay time is set by $\tau_1$. $\tau_2$ is calculated via the relationship $\tau_{rise} = \tau_1\tau_2/(\tau_2 - \tau_1)$. This impulse response reaches its maximum at time $\ln(\tau_1/\tau_2) \cdot$

$\tau_{rise}$. Similarly to the case of alpha function, the convolution by $h_m$ can be written in the form of a differential equation:

$$\ddot{s}_{mk} = B(\tau_2^{-1} - \tau_1^{-1})N_{k'k} \cdot Q_{k'}(V_{k'}) - \tau_2^{-1}\tau_1^{-1}s_{mk} - (\tau_2^{-1} + \tau_1^{-1})\dot{s}_{mk} \tag{17}$$

The 'two-exponential' assumption of synaptic kinetics captures more characteristics, but induce one more parameter. Therefore, to limit the number of unknown parameters, we model all synapses with precisely-reported time constants with the 'two-exponential' framework but confine unknwon synapses within the alpha function framework.

For synapses with long-distance projections across brain regions (e.g. thalamocortical projection), following the original paper, we deal with the axonal conductance delay by adding another linear filter of the synaptic output, which can be approximated by the convolution of another alpha function:

$$\ddot{\phi}_k = \nu^2 \cdot (Q_k(V_k) - \phi_k) - 2 \cdot \dot{\phi}_k \tag{18}$$

## Membrane potential and local field potential (LFP)

The final step is to establish how the membrane potential evolves with the transmembrane currents. The neuron population is assumed equivalent to a neuron modelled with a single compartment model. As illustrated in Fig. 1, the most simplified case is a neuron population $k$ influenced by a single ($m$-type) synaptic current $J_m^k(s_{mk})$ and a single intrinsic current $I_i$.

The denoted synaptic conductance follows the representation in Eq. 10. With Kirchhoff's current law, we would be able to get the adaptation of membrane potential $V_k$ with currents:

$$C_m\dot{V}_k = -\frac{V_k - E_L}{R_L} - g_{mk}(s_{mk}) \cdot (V_k - E_L) - I_i \tag{19}$$

The second term on the right in Eq. 19 represents the synaptic current, where $g_{mk}(s_{mk})$ is the real synaptic conductance. Comparing this form with the synaptic current model (Eq. 9, 10), the synaptic conductance $s_{mk} \cdot g(V_k)$ can be seen as the real conductance $g_{mk}(s_{mk})$ normalized by the leaky conductance $1/R_L$, i.e.

$$s_{mk} \cdot g(V_k) = \frac{g_{mk}(s_{mk})}{1/R_L} \Rightarrow g_{mk}(s_{mk}) = \frac{s_{mk} \cdot g(V_k)}{R_L} \tag{20}$$

Thus combining Eq. 9, 10, Eq. 19 can be rewritten as:

$$C_m\dot{V}_k = -\frac{V_k - E_L}{R_L} - \frac{J_m^k(s_{mk})}{R_L} - I_i \tag{21}$$

By rearranging the denominator, we can obtain:

$$R_L \cdot C_m\dot{V}_k = -(V_k - E_L) - J_m^k(s_{mk}) - R_L \cdot I_i \tag{22}$$

The first term on the right in Eq. 22 can be understood as another equivalent current $J_L^k$ that passes through the membrane. $J_L^k = (V_k - E_L^k)$ is defined as the general leaky current, a linear current unaffected by either presynaptic or postsynaptic population. Note the $K^+$ leaky current is excluded because we mentioned in Section Cholinergic modulation of PGO waves that it is influenced by the concentration of ACh.

In experiments a commonly reported feature is the membrane time constant $\tau_k = R_L \cdot C_m$. With a rearrangement of terms, Eq. 22 can be written as:

$$\tau_k\dot{V}_k = -J_L^k - J_m^k(s_{mk}) - C_m^{-1} \cdot \tau_k \cdot I_i \tag{23}$$

In more general cases, the numbers of synaptic as well as intrinsic currents are not necessarily confined to one. For multiple currents we can obtain the general form:

$$\tau_k\dot{V}_k = -J_L^k - \sum_{m,k} J_m^k(s_{mk}) - C_m^{-1}\tau_k \sum_i I_i \tag{24}$$

In many experimental studies, the thalamic PGO waves are often characterized in LFPs. LFPs reflect some spatially extended measure of the activities of a mass of neurons. While understanding of the nature of LFPs is still preliminary, one study attempted to link LFP with the currents flowing through the neuron populations (Mazzoni et al., 2015). In this study the authors approximate the LFP with a weighted sum of synaptic currents, e.g. AMPA and GABA currents, which is to some extent compatible with our model. However, in our model the intrinsic currents also play important roles. We propose to model the LFP of a neuron population as a instantaneous sum of all currents to take into account the effects of intrinsic current:

$$LFP_k = -J_L^k - \sum_{m,k} J_m^k(s_{mk}) - \sum_i I_i \tag{25}$$

## Model assumption for the pons

Two groups of neurons in the pontine region, termed as the PGO *triggering neurons* and *transferring neurons*, are the executive elements of PGO waves (Datta, 1997). They are both located in the peribrachial area (PBL) (Silvestri and Kapp, 1998), which contains a number of important nuclei that are involved in regulation of sleep and arousal. Functionally, the PBL can be separated into two parts: the rostal (R-PBL) and the caudolateral (C-PBL) parts (Datta, 1997). The R-PBL mainly consists of the pedunculopontine tegmentum (PPT) nucleus and laterodorsal tegmentum (LDT) nucleus, while the most important nuclei in C-PBL include the parabrachial nucleus.

As their name indicates, experimental evidence showed that triggering neurons are PGO-state-on bursting neurons assumed to initiate the PGO phasic event located in C-PBL (Datta and Hobson, 1994; Datta, 1995, 1997). PGO triggering neurons were recorded to burst in high frequency (300-500Hz) $25 \pm 7$ ms before the thalamic PGO waves. These activities are hypothesized to propagate to the so-called transferring neurons in R-PBL, which are PGO-on low-frequency bursting neurons (Datta, 1997) firing low-frequency ($120$-$180Hz$) bursts with 3-5 spikes $5$-$15ms$ before the thalamic PGO waves (McCarley et al., 1978; Nelson et al., 1983; Steriade et al., 1990; Sakai and Jouvet, 1980). The transferring neurons were presumed to project directly to the thalamus (Sakai and Jouvet, 1980) as the last relay station of the local PGO-related circuits in the pons (Paré et al., 1990).

In the model, C-PBL activities (of the triggering neurons) is assumed as a trigger that initializes the whole network activity. To match the high-frequency bursts pooled across a population, the firing rate of C-PBL neurons should rise rapidly and persist for a short period. It is then natural to model the C-PBL activity in pre-REM stage as a brief pulse lasting $10ms$ as an approximation of the bursts duration (Datta and Hobson, 1994). Deducing from experimentally-reported peri-PGO spike histograms (Datta and Hobson, 1994), we assume that REM-related C-PBL bursts can be modelled by three $10 - ms$ pulses with a bursting interval of $200ms$.

The R-PBL PGO-transferring neuron populations are modelled with the same type of sigmoidal activation function as for the thalamic neurons (Eq. 2). The activation threshold remain unchanged because the pontine and thalamic spikings are both associated with fast $Na^{2+}$ spikes and should match each other. We present briefly here the synaptic connection from C-PBL neurons to R-PBL neurons and some intrinsice cellular mechanisms of R-PBL neurons.

The projection from triggering neurons to transferring neurons is presumably glutamatergic (Inglis and Semba, 1996; Sanchez and Leonard, 1994, 1996; Datta, 2012), indirectly supported by the findings that other neurotransmitters are inhibitory (Luebke et al., 1992; Leonard and Llinás, 1994; Williams and Reiner, 1993). Electrophysiological studies showed the projection could be mediated by a combination of NMDA and AMPA receptors (Sanchez and Leonard, 1996), with a contribution ratio as NMDA:AMPA = 1:5. The same experiment also quantified the decay times for both currents: 8.77ms for the AMPA channel and 129.4ms for for NMDA. The Nernst potentials were measured to be 16.3mV for NMDA and 3.4mV for AMPA (close to the theoretical value 0mV).

Conductance of the AMPA channel is invariant to the postsynaptic membrane potential. Nonlinearity in NMDA currents has long been reported and well-documented. We followed the classical

modelling of the voltage dependence first introduced by Destexhe ((Destexhe et al., 1994)):

$$g_{NMDA}(V_l) = \frac{1}{1+\exp(-0.0062V_l)}[Mg^{2+}]_o/3.57 \tag{26}$$

where $l$ represents the population of R-PBL transferring neurons, and $V_l$ denotes its membrane potential. $[Mg]_o$ represents the extracellular concentration for $Mg^{2+}$ ions.

The slow-frequency bursts occuring in transferring neurons are rebound bursts evoked by activating an intrinsic low-threshold calcium T-current under hyperpolarization (Kang and Kitai, 1990; Kamondi et al., 1992). As it is similar to the thalamic T-currents discovered in the TC neurons, we modelled it with Eq. 5 (Destexhe et al., 1998, 1994), but refitted the conductance with digitized experimental I-V curves (Kamondi et al., 1992). We constructed a Boltzmann-like function that is able to approximate the activation curve:

$$m^l_\infty(V_l) = \frac{2}{1+\exp(-(V_l+50.6/0.44)+\exp((V_l+50.6/17.4} \tag{27}$$

In a similar way, we fitted the inactivation gating variable leading to:

$$h^l_\infty(V_l) = \frac{1}{1+\exp((V_l+65)/2.7)} \tag{28}$$

Considering the increasing concentration of ACh during PGO-related sleep stages, together with evidence of the inhibitory effects of Ach on transferring neurons (Leonard and Llinás, 1994), we assume that some cholinergic modulatory inputs causes the hyperpolarization as a prerequisite to de-inactivate the T-current. The cholinergic input goes through a potassium inward rectifier mediated by a muscarinic receptor (Leonard and Llinás, 1994). The I-V curve of cholinergic influence has already been characterized, from which we defined an approximate mathematical formulation with a procedure similar to the fitting of T-currents.

$$g_{IR}(V_l) = \frac{1}{1+\exp((V_l+35)/10.9)} \tag{29}$$

## Propagation of pontine PGO waves to the thalamus

The complete model involving carefully-designed ponto-thalamic synaptic connections is illustrated in Fig. **??**. After receiving bursting activities from the triggering neurons, the transferring neurons send cholinergic inputs to the three thalamic neurons (TC and RT neurons and LGin neurons) via 5 cholinergic ponto-thalamic projections. Here we briefly present our assumptions regarding the chemical nature and kinetics of the pontine-thalamic projections and neurophysiological evidence supporting them.

The R-PBL neurons send two excitatory projections to the TC neurons via cholinergic projections mediated by both nAChR and mAChR receptors. The nAChR-based channel, underlying the generation mechanism of a fast depolarization in diafferated cats (McCormick and Prince, 1987b; Hu et al., 1988, 1989a,a) and short bursting in naturally sleeping cats (Steriade et al., 1989; McCormick and Prince, 1987b; Hu et al., 1989b), let through a mixed cation current with a voltage-independent conducatance and a Nernst potential of $18.9 \pm 8.9mV$ (McCormick and Prince, 1987b). The mAChR-mediated synapse, generating the prolonged spiking in TC neurons following the initial bursts, is coupled to a leaky $K^+$ channel via G-protein cascade (reversal potential: $-97 \pm 6.1mV$, note that "leaky" implies a voltage-independent conductance) (McCormick, 1992). We set the conductance negative as activation of the mAChR-mediated synapse decreases the conductance (i.e. closes the channel). Specifically, we speculate that this potassium leaky channel is the same channel as the $K^+$ leaky channel already included in the original model of TC neurons (see Section Intrinsic currents and Section Cholinergic modulation of PGO waves), whose role is designed to mediate membrane de-/hyperpolarization (McCormick and Prince, 1987b; Bista et al., 2012, 2015). We introduced a saturation mechanism: the maximum amount of conductance decrease caused by the mAChR-mediated synapse is equal to its resting conductance, i.e. it cannot go beyond complete

closure. This saturation mechanism was not reported but implied in the experimental papers, and has been proven useful in replicating the switch between PGO wave subtypes (see Fig. 1).

Clear evidence suggests that the RT neurons also receive pontine inputs via both nAChR- and mAChR-mediated synapses, corresponding to a PGO-triggered fast depolarization/bursting and slow hyperpolarization observed in RT neurons (Hu et al., 1989a; Lee and McCormick, 1995; Oda et al., 2007; Sun et al., 2013; Beierlein, 2014). The time constants of synatic kinetics were quantified (rise time: $10.8ms$, decay time: $123.6ms$), enabling us to apply the 'two-exponential' form of synaptic model. Following classical models of nAChR-mediated channels, we assume a linear voltage-independent with a reversal potential of $-5mV$. On the contrary, the mAChR-regulated channel, associated with a $K^+$ channel with the Nernst potential of around $-93.2 \pm 0.6mV$ (Sun et al., 2013), works as a inward rectifier (Hu et al., 1989a; Oda et al., 2007; Lee and McCormick, 1995; Sun et al., 2013; Beierlein, 2014), whose conductance decreases with increased membrane potential, with voltage dependence characterized and fitted with asigmoidal function:

$$g_{mAChR}(V_r) = \frac{1}{1 + \exp((V_r + 66.3)/29.1)} \tag{30}$$

The corresponding rise time and decay time of the synaptic kinetics are $107.6 \pm 8.6ms$ and $639.0 \pm 102ms$.

The assumption that LGin neurons contribute to thalamic PGO wave generation is supported by the existence of a transient hyperpolarization of TC neurons caused by depolarization in LGin neurons (Hu et al., 1989a,b,c; Steriade et al., 1989). We model a nAChR-mediated projection from R-PBL neurons to LGin neurons to generate the depolarization (Zhu et al., 1999), with the same model as the corresponding channel in TC neurons with differently-tuned synaptic kinetics. Conservatively, for simplicity we omit the other potentially existing instrinsic current, as current experimental evidence is insufficient to support their roles in thalamic PGO wave formation.

The transmission of PGO-related activities from pons to the thalamus is not instataneous but delayed by membrane and axonal properties. For the 5 pontine-thalamic connections, the only precisely reported fact is the latency difference between nAChR-mediated and mAChR-mediated currents in RT neurons, as $28ms$ (Sun et al., 2013). Latency histograms of the nAChR-mediated currents in TC and RT neurons (Hu et al., 1989c) also suggest a constraint in setting the delays. Extrapolating with all taken into consideration, we implement the delays in our model by setting a fixed latency for each projection that is consistent with the experimentally-revealed facts.

## Cholinergic modulation of PGO waves

Transition from pre-REM to REM sleep stages is strongly dependent on the changes of certain neuromodulators (Datta, 1997). To reproduce the difference between PGO wave subtypes during pre-REM and REM, we need to know how neuromodulation affects the PGO propagating network.

Modulatory neuron populations associated with ACh and monoamines (serotonin (5-HT) and noradrenaline (NE)) are reciprocally interacting to influence the activities of the several neuron types related to PGO wave generation (Hobson, 2009). Wakefulness and non-REM sleep is accompanied with high concentration of monoamines and low concentration of ACh. In the transitional stage (i.e. pre-REM), the activities of aminergic neurons decrease while the cholinergic neurons are gradually activated. When REM sleep is approached, cholinergic activities remain persistently in high level whereas aminergic activities are suppressed. In short, aminergic neurons plays a disinhibitory gating role for the cholinergic neurons, i.e. activities of the former is negatively correlated with the latter. Thus for simplicity we can omit the monoamines and model only the effect of ACh on the network activities.

The levels of acetylcholine concentration in the pons and in the thalamus are mainly influenced by the cholinergic tonic firing neurons in the R-PBL which directly project to both thalamic nuclei. From non-REM to REM states, these neurons continuously increase their firing rates (Steriade et al., 1990). We use this observation to build a simple linear approximation of the transition between the two states depending on the normalized ACh concentration $[ACh](t)$ (ranging from 0 to 1).

Our strategies of linking ACh concentration to the activity patterns of PGO-related neurons are as follows:

- First, pick several crucial parameters in the model based on biological plausibility (e.g. maximum conductance for currents or activation threshold of neuronal populations), which were reported to contribute to the switch from non-REM sleep to REM sleep.
- Next, adjust and fix these parameters to reproduce the firing modes of neurons in pre-REM and REM states.
- Finally, establish a sigmoidal relationship between the ACh concentration and the crucial parameters based on experimental evidence, i.e. highest ACh concentration during REM and lowest during pre-REM.

For the cortex, the state-reconstruction can resolved by simplifying the neuromodulated isolated cortical model in Costa et al. (2016): instead of modulating the cortical network with the concentrations of ACh, serotonin and noradrenaline, we restrict the neuromodulation to ACh. As for the cortical 'critical parameters', we followed their choice of the adaptation strength of the sodium-dependent potassium current $\bar{g}_{KNa}$, but changed the other to the maximum firing rate of Pyr neurons $Q_p^{max}$ (Barkai and Hasselmo, 1994; Disney et al., 2007; Soma et al., 2012; Steriade et al., 2001) to ensure a broader range of REM activities.

ACh has been reported in vitro and in vivo to tonically depolarize TC neurons (McCormick and Prince, 1987a; Deschênes and Hu, 1990; Steriade et al., 1993b) and hyperpolarize RT neurons , both via a mAChR-mediated $K^+$ channels (Varela and Sherman, 2007; McCormick and Prince, 1987a; Varela, 2014). State transitions in the thalamus is implemented by modulating the $K^+$ leaky conductance present in the model of both TC and RT neurons, as described in Section Intrinsic currents.

For TC neurons, we decreased its potassium leaky conductance conductance from 0.24 to 0.06 to mimick its depolarization. The same conductance in RT neurons was increased from 0.18 to 0.62 to simulate the hyperpolarization. The values of conductance are optimal parameter according empirical experience of tuning the dynamic system, whereas various other combinations would also satisfy the requirements for state switches.

While some related studies (McCormick and Prince, 1987a; Deschênes and Hu, 1990; Zhu and Uhlrich, 1998), measuring how much the leaky conductance was changed in response to ACh application, might have provided a quantitative basis for setting the conductance values, we did not follow them because many unknown experimental variables (in vivo/in vitro, anesthesia, doses of micro-injections, etc.) lead to large uncertainty on the parameter choice.

## Pontine parameter tuning

The quantitative match observed in Supplementary Fig. 1A results from appropriate adjustment of the conductance of the hyperpolarizing current in R-PBL neurons, which control its bursting behavior. The cellular mechanisms at play and resulting parameter choice are illustrated in Supplementary Fig. 1C. Bursting activities are co-activated by a low-threshold calcium T-current (Kang and Kitai, 1990; Kamondi et al., 1992; Leonard, 1990) and a hyperpolarizing mAChR-mediated intrinsic cholinergic current (Leonard and Llinás, 1994). The low-threshold T-current, similar to the standard T-current discovered in the thalamus and fitted on rat electrophysiological data, is activated only upon resting hyperpolarization and a fast depolarizing input (for details see Methods, section Model assumption for the pons). The conductance of the cholinergic intrinsic currents regulates the degree of hyperpolarization in the resting potential of R-PBL neurons. As shown in Fig. 1, with a fixed strength of synaptic input from C-PBL neurons, only a carefully selected range of cholinergic conductance is able to trigger a calcium spike with bursts; too strong or weak resting hyperpolarization only cause a small depolarizing effect but no bursts. Therefore, based on such nonlinear properties, we are able to find an appropriate value of the cholinergic conductance to achieve the biologically-based temporal characteristics of pontine activity reported in Supplementary Table 1.

### Validation of Ponto-thalamic projections

We consider one projection necessary if the PGO waveforms generated with it can not be reproduced in its absence, regardless of the variation of the other projections. In practice, this can be verified by using a dimensionality reduction technique mapping each shape to a point in a 2-dimensional space, and checking whether the waveforms simulated with and without each projection map to distinct regions of this space.

We thus complement the dataset of the original PGO waveforms generated with full ponto-thalamic projections (which underlies the Fig. 1 and Fig. 3) with 5 datasets of 500 substitute PGO waveforms by blocking each of the ponto-thalamic projections. Blockade is implemented by setting the corresponding projection strength to zero, while the strength of unblocked projections are set to randomly deviate maximally 100% from the optimized values. We assume that the range of parameter variations is large enough to cover most of the parameter space for the generation of PGO waveforms. From these 6 datasets we take as features the waveforms of population membrane potential, firing rates and LFPs, separately for pre-REM and REM states. We reduce the high-dimensional features into 2 dimensions by applying T-SNE which has been shown to perform well on dimension reduction problems of time series (Maaten and Hinton, 2008). The point clouds in Fig. 2 show the REM features of the optimized PGO waveforms with full projections are clearly separated from the 5 blockade conditions, although not during pre-REM states, which is enough to indicate that each of the ponto-thalamic projections has a specific role in the generation of PGO-related waveforms.

#### Python implementation

All simulation were implemented in the Python package ANNarchy[1] (acronym for Artificial Neural Networks architect).

## References

Barkai, E. and Hasselmo, M. E. (1994). Modulation of the input/output function of rat piriform cortex pyramidal cells. *Journal of Neurophysiology*, 72(2):644–658.

Beierlein, M. (2014). Synaptic mechanisms underlying cholinergic control of thalamic reticular nucleus neurons. *The Journal of Physiology*, 592(19):4137–4145.

Bi, G. Q. and Poo, M. M. (1998). Synaptic modifications in cultured hippocampal neurons: dependence on spike timing, synaptic strength, and postsynaptic cell type. *The Journal of Neuroscience*, 18(24):10464–10472.

Bista, P., Cerina, M., Ehling, P., Leist, M., Pape, H.-C., Meuth, S. G., and Budde, T. (2015). The role of two-pore-domain background $k^+$ ($k_2$p) channels in the thalamus. *Pflugers Archiv: European Journal of Physiology*, 467(5):895–905.

Bista, P., Meuth, S. G., Kanyshkova, T., Cerina, M., Pawlowski, M., Ehling, P., Landgraf, P., Borsotto, M., Heurteaux, C., Pape, H.-C., Baukrowitz, T., and Budde, T. (2012). Identification of the muscarinic pathway underlying cessation of sleep-related burst activity in rat thalamocortical relay neurons. *Pflugers Archiv: European Journal of Physiology*, 463(1):89–102.

Bizzi, E. (1966). Discharge patterns of single geniculate neurons during the rapid eye movements of sleep. *Journal of Neurophysiology*, 29(6):1087–1095.

Bowker, R. M. (1985). Variability in the characteristics of pontogeniculooccipital spikes during paradoxical sleep. *Experimental Neurology*, 87(2):212–224.

Boyce, R., Glasgow, S. D., Williams, S., and Adamantidis, A. (2016). Causal evidence for the role of REM sleep theta rhythm in contextual memory consolidation. *Science*, 352(6287):812–816.

Boyce, R., Williams, S., and Adamantidis, A. (2017). REM sleep and memory. *Current Opinion in Neurobiology*, 44:167–177.

[1] https://www.tu-chemnitz.de/informatik/KI/projects/ANNarchy/index.php

Brooks, D. C. (1968). Waves associated with eye movement in the awake and sleeping cat. *Electroencephalography and Clinical Neurophysiology*, 24(6):532–541.

Buzsáky, G. (1998). Memory consolidation during sleep: a neurophysiological perspective. *Journal of sleep research*, 7(S1):17–23.

Callaway, C. W., Lydic, R., Baghdoyan, H. A., and Hobson, J. A. (1987). Pontogeniculooccipital waves: spontaneous visual system activity during rapid eye movement sleep. *Cellular and Molecular Neurobiology*, 7(2):105–149.

Cohen, B. and Feldman, M. (1968). Relationship of electrical activity in pontine reticular formation and lateral geniculate body to rapid eye movements. *Journal of Neurophysiology*, 31(6):806–817.

Costa, M. S., Born, J., Claussen, J. C., and Martinetz, T. (2016). Modeling the effect of sleep regulation on a neural mass model. *Journal of Computational Neuroscience*, 41(1):15–28.

Datta, S. (1995). Neuronal activity in the peribrachial area: relationship to behavioral state control. *Neuroscience and Biobehavioral Reviews*, 19(1):67–84.

Datta, S. (1997). Cellular basis of pontine ponto-geniculo-occipital wave generation and modulation. *Cellular and Molecular Neurobiology*, 17(3):341–365.

Datta, S. (2000). Avoidance task training potentiates phasic pontine-wave density in the rat: A mechanism for sleep-dependent plasticity. *The Journal of Neuroscience*, 20(22):8607–8613.

Datta, S. (2012). Phasic pontine-wave (p-wave) generation. In *Sleep and brain activity*, pages 147–164. Elsevier.

Datta, S., Calvo, J., Quattrochi, J., and Hobson, J. (1992). Cholinergic microstimulation of the peribrachial nucleus in the cat. i. immediate and prolonged increases in ponto-geniculo-occipital waves. *Archives italiennes de biologie*, 130(4):263.

Datta, S. and Hobson, J. A. (1994). Neuronal activity in the caudolateral peribrachial pons: relationship to PGO waves and rapid eye movements. *Journal of Neurophysiology*, 71(1):95–109.

Datta, S. and Hobson, J. A. (1995). Suppression of ponto-geniculo-occipital waves by neurotoxic lesions of pontine caudo-lateral peribrachial cells. *Neuroscience*, 67(3):703–712.

Datta, S., Mavanji, V., Patterson, E. H., and Ulloor, J. (2003). Regulation of rapid eye movement sleep in the freely moving rat: local microinjection of serotonin, norepinephrine, and adenosine into the brainstem. *Sleep*, 26(5):513–520.

Datta, S., Mavanji, V., Ulloor, J., and Patterson, E. H. (2004). Activation of phasic pontine-wave generator prevents rapid eye movement sleep deprivation-induced learning impairment in the rat: a mechanism for sleep-dependent plasticity. *The Journal of Neuroscience*, 24(6):1416–1427.

Datta, S. and O'Malley, M. W. (2013). Fear extinction memory consolidation requires potentiation of pontine-wave activity during REM sleep. *The Journal of Neuroscience*, 33(10):4561–4569.

Datta, S., Siwek, D. F., Patterson, E. H., and Cipolloni, P. B. (1998). Localization of pontine PGO wave generation sites and their anatomical projections in the rat. *Synapse*, 30(4):409–423.

Deboer, T., Ross, R. J., Morrison, A. R., and Sanford, L. D. (1999). Electrical stimulation of the amygdala increases the amplitude of elicited ponto-geniculo-occipital waves. *Physiology & Behavior*, 66(1):119–124.

Deboer, T., Sanford, L. D., Ross, R. J., and Morrison, A. R. (1998). Effects of electrical stimulation in the amygdala on ponto-geniculo-occipital waves in rats. *Brain Research*, 793(1-2):305–310.

Deschênes, M. and Hu, B. (1990). Membrane resistance increase induced in thalamic neurons by stimulation of brainstem cholinergic afferents. *Brain Research*, 513(2):339–342.

Destexhe, A., Bal, T., McCormick, D. A., and Sejnowski, T. J. (1996). Ionic mechanisms underlying synchronized oscillations and propagating waves in a model of ferret thalamic slices. *Journal of Neurophysiology*, 76(3):2049–2070.

Destexhe, A., Contreras, D., Sejnowski, T. J., and Steriade, M. (1994). A model of spindle rhythmicity in the isolated thalamic reticular nucleus. *Journal of Neurophysiology*, 72(2):803–818.

Destexhe, A., Neubig, M., Ulrich, D., and Huguenard, J. (1998). Dendritic low-threshold calcium currents in thalamic relay cells. *The Journal of Neuroscience*, 18(10):3574–3588.

Diekelmann, S. and Born, J. (2010). The memory function of sleep. *Nature Reviews. Neuroscience*, 11(2):114–126.

Disney, A. A., Aoki, C., and Hawken, M. J. (2007). Gain modulation by nicotine in macaque v1. *Neuron*, 56(4):701–713.

Einevoll, G. T., Kayser, C., Logothetis, N. K., and Panzeri, S. (2013). Modelling and analysis of local field potentials for studying the function of cortical circuits. *Nature Reviews. Neuroscience*, 14(11):770–785.

Fernández-Mendoza, J., Lozano, B., Seijo, F., Santamarta-Liébana, E., Ramos-Platón, M. J., Vela-Bueno, A., and Fernández-González, F. (2009). Evidence of subthalamic PGO-like waves during REM sleep in humans: a deep brain polysomnographic study. *Sleep*, 32(9):1117–1126.

Fung, P. K. and Robinson, P. A. (2013). Neural field theory of calcium dependent plasticity with applications to transcranial magnetic stimulation. *Journal of Theoretical Biology*, 324:72–83.

Gott, J. A., Liley, D. T. J., and Hobson, J. A. (2017). Towards a functional understanding of PGO waves. *Frontiers in Human Neuroscience*, 11:89.

Gridchyn, I., Schoenenberger, P., O'Neill, J., and Csicsvari, J. (2020). Assembly-specific disruption of hippocampal replay leads to selective memory deficit. *Neuron*.

Grosmark, A. D., Mizuseki, K., Pastalkova, E., Diba, K., and Buzsáki, G. (2012). REM sleep reorganizes hippocampal excitability. *Neuron*, 75(6):1001–1007.

Hobson, J. A. (1965). The effects of chronic brain-stem lesions on cortical and muscular activity during sleep and waking in the cat. *Electroencephalography and Clinical Neurophysiology*, 19:41–62.

Hobson, J. A. (2009). REM sleep and dreaming: towards a theory of protoconsciousness. *Nature Reviews. Neuroscience*, 10(11):803–813.

Hu, B., Bouhassira, D., Steriade, M., and Deschênes, M. (1988). The blockage of ponto-geniculo-occipital waves in the cat lateral geniculate nucleus by nicotinic antagonists. *Brain Research*, 473(2):394–397.

Hu, B., Steriade, M., and Deschênes, M. (1989a). The cellular mechanism of thalamic ponto-geniculo-occipital waves. *Neuroscience*, 31(1):25–35.

Hu, B., Steriade, M., and Deschênes, M. (1989b). The effects of brainstem peribrachial stimulation on neurons of the lateral geniculate nucleus. *Neuroscience*, 31(1):13–24.

Hu, B., Steriade, M., and Deschênes, M. (1989c). The effects of brainstem peribrachial stimulation on perigeniculate neurons: the blockage of spindle waves. *Neuroscience*, 31(1):1–12.

Inglis, W. L. and Semba, K. (1996). Colocalization of ionotropic glutamate receptor subunits with NADPH-diaphorase-containing neurons in the rat mesopontine tegmentum. *The Journal of Comparative Neurology*, 368(1):17–32.

Jansen, B. H., Zouridakis, G., and Brandt, M. E. (1993). A neurophysiologically-based mathematical model of flash visual evoked potentials. *Biological Cybernetics*, 68(3):275–283.

Jouvet, M. (1959). Correlations electromyographiques du sommeil chez le chat decortique et mesencephalique chronique. *C. R. Soc. Biol.*

Kamondi, A., Williams, J. A., Hutcheon, B., and Reiner, P. B. (1992). Membrane properties of mesopontine cholinergic neurons studied with the whole-cell patch-clamp technique: implications for behavioral state control. *Journal of Neurophysiology*, 68(4):1359–1372.

Kang, Y. and Kitai, S. T. (1990). Electrophysiological properties of pedunculopontine neurons and their postsynaptic responses following stimulation of substantia nigra reticulata. *Brain Research*, 535(1):79–95.

Kaufman, L. S. and Morrison, A. R. (1981). Spontaneous and elicited PGO spikes in rats. *Brain Research*, 214(1):61–72.

Klinzing, J. G., Niethard, N., and Born, J. (2019). Mechanisms of systems memory consolidation during sleep. *Nature Neuroscience*.

Krishnan, G. P., Chauvette, S., Shamie, I., Soltani, S., Timofeev, I., Cash, S. S., Halgren, E., and Bazhenov, M. (2016). Cellular and neurochemical basis of sleep stages in the thalamocortical network. *eLife*, 5.

Latchoumane, C.-F. V., Ngo, H.-V. V., Born, J., and Shin, H.-S. (2017). Thalamic spindles promote memory formation during sleep through triple phase-locking of cortical, thalamic, and hippocampal rhythms. *Neuron*, 95(2):424–435.e6.

Lee, K. H. and McCormick, D. A. (1995). Acetylcholine excites GABAergic neurons of the ferret perigeniculate nucleus through nicotinic receptors. *Journal of Neurophysiology*, 73(5):2123–2128.

Leonard, C. S. and Llinás, R. (1994). Serotonergic and cholinergic inhibition of mesopontine cholinergic neurons controlling REM sleep: an in vitro electrophysiological study. *Neuroscience*, 59(2):309–330.

Leonard, S. (1990). Electrophysiology of mammalian pedunculopontine and laterodorsal tegmental neurons in vitro: Implications for the control of REM sleep. *Brain Cholinergic System*.

Levenstein, D., Buzsáki, G., and Rinzel, J. (2019). NREM sleep in the rodent neocortex and hippocampus reflects excitable dynamics. *Nature Communications*, 10(1):2478.

Levenstein, D., Watson, B. O., Rinzel, J., and Buzsáki, G. (2017). Sleep regulation of the distribution of cortical firing rates. *Current Opinion in Neurobiology*, 44:34–42.

Li, W., Ma, L., Yang, G., and Gan, W.-B. (2017). REM sleep selectively prunes and maintains new synapses in development and learning. *Nature Neuroscience*, 20(3):427–437.

Lim, A. S., Lozano, A. M., Moro, E., Hamani, C., Hutchison, W. D., Dostrovsky, J. O., Lang, A. E., Wennberg, R. A., and Murray, B. J. (2007). Characterization of REM-sleep associated ponto-geniculo-occipital waves in the human pons. *Sleep*, 30(7):823–827.

Lopes da Silva, F. H., Hoeks, A., Smits, H., and Zetterberg, L. H. (1974). Model of brain rhythmic activity. *Kybernetik*, 15(1):27–37.

Luebke, J. I., Greene, R. W., Semba, K., Kamondi, A., McCarley, R. W., and Reiner, P. B. (1992). Serotonin hyperpolarizes cholinergic low-threshold burst neurons in the rat laterodorsal tegmental nucleus in vitro. *Proceedings of the National Academy of Sciences of the United States of America*, 89(2):743–747.

Maaten, L. v. d. and Hinton, G. (2008). Visualizing data using t-sne. *Journal of machine learning research*, 9(Nov):2579–2605.

Maingret, N., Girardeau, G., Todorova, R., Goutierre, M., and Zugaro, M. (2016). Hippocampo-cortical coupling mediates memory consolidation during sleep. *Nature Neuroscience*, 19(7):959–964.

Mavanji, V. and Datta, S. (2003). Activation of the phasic pontine-wave generator enhances improvement of learning performance: a mechanism for sleep-dependent plasticity. *The European Journal of Neuroscience*, 17(2):359–370.

Mazzoni, A., Lindén, H., Cuntz, H., Lansner, A., Panzeri, S., and Einevoll, G. T. (2015). Computing the local field potential (LFP) from integrate-and-fire network models. *PLoS Computational Biology*, 11(12):e1004584.

McCarley, R. W., Nelson, J. P., and Hobson, J. A. (1978). Ponto-geniculo-occipital (PGO) burst neurons: correlative evidence for neuronal generators of PGO waves. *Science*, 201(4352):269–272.

McCormick, D. A. (1992). Cellular mechanisms underlying cholinergic and noradrenergic modulation of neuronal firing mode in the cat and guinea pig dorsal lateral geniculate nucleus. *The Journal of Neuroscience*, 12(1):278–289.

McCormick, D. A. and Bal, T. (1997). Sleep and arousal: thalamocortical mechanisms. *Annual Review of Neuroscience*, 20:185–215.

McCormick, D. A. and Pape, H. C. (1988). Acetylcholine inhibits identified interneurons in the cat lateral geniculate nucleus. *Nature*, 334(6179):246–248.

McCormick, D. A. and Prince, D. A. (1986). Acetylcholine induces burst firing in thalamic reticular neurones by activating a potassium conductance. *Nature*, 319(6052):402–405.

McCormick, D. A. and Prince, D. A. (1987a). Acetylcholine causes rapid nicotinic excitation in the medial habenular nucleus of guinea pig, in vitro. *The Journal of Neuroscience*, 7(3):742–752.

McCormick, D. A. and Prince, D. A. (1987b). Actions of acetylcholine in the guinea-pig and cat medial and lateral geniculate nuclei, in vitro. *The Journal of Physiology*, 392:147–165.

McDevitt, E. A., Duggan, K. A., and Mednick, S. C. (2015). REM sleep rescues learning from interference. *Neurobiology of Learning and Memory*, 122:51–62.

Morrison, A. R. and Pompeiano, O. (1966). Vestibular influences during sleep. II. effects of vestibular lesions on the pyramidal discharge during desynchronized sleep. *Archives Italiennes de Biologie*, 104(2):214–230.

Muller, L. and Destexhe, A. (2012). Propagating waves in thalamus, cortex and the thalamocortical system: experiments and models. *Journal of Physiology-Paris*, 106(5-6):222–238.

Nelson, J. P., McCarley, R. W., and Hobson, J. A. (1983). REM sleep burst neurons, PGO waves, and eye movement information. *Journal of Neurophysiology*, 50(4):784–797.

Niethard, N., Ngo, H.-V. V., Ehrlich, I., and Born, J. (2018). Cortical circuit activity underlying sleep slow oscillations and spindles. *Proceedings of the National Academy of Sciences of the United States of America*, 115(39):E9220–E9229.

Oda, S., Sato, F., Okada, A., Akahane, S., Igarashi, H., Yokofujita, J., Yang, J., and Kuroda, M. (2007). Immunolocalization of muscarinic receptor subtypes in the reticular thalamic nucleus of rats. *Brain Research Bulletin*, 74(5):376–384.

Paré, D., Curró Dossi, R., Datta, S., and Steriade, M. (1990). Brainstem genesis of reserpine-induced ponto-geniculo-occipital waves: an electrophysiological and morphological investigation. *Experimental Brain Research*, 81(3):533–544.

Puentes-Mestril, C., Roach, J., Niethard, N., Zochowski, M., and Aton, S. J. (2019). How rhythms of the sleeping brain tune memory and synaptic plasticity. *Sleep*, 42(7).

Ramirez-Villegas, J. F., Besserve, M., Murayama, Y., Evrard, H. C., Oeltermann, A., and Logothetis, N. K. (2020). Coupling of hippocampal theta and ripples with pontogeniculooccipital waves. *Nature*.

Robinson, P. A. (2011). Neural field theory of synaptic plasticity. *Journal of Theoretical Biology*, 285(1):156–163.

Sakai, K. and Jouvet, M. (1980). Brain stem PGO-on cells projecting directly to the cat dorsal lateral geniculate nucleus. *Brain Research*, 194(2):500–505.

Sanchez, R. and Leonard, C. S. (1994). NMDA receptor-mediated synaptic input to nitric oxide synthase-containing neurons of the guinea pig mesopontine tegmentum in vitro. *Neuroscience Letters*, 179(1-2):141–144.

Sanchez, R. and Leonard, C. S. (1996). NMDA-receptor-mediated synaptic currents in guinea pig laterodorsal tegmental neurons in vitro. *Journal of Neurophysiology*, 76(2):1101–1111.

Sanchez-Vives, M. V. and McCormick, D. A. (2000). Cellular and network mechanisms of rhythmic recurrent activity in neocortex. *Nature Neuroscience*, 3(10):1027–1034.

Schellenberger Costa, M., Weigenand, A., Ngo, H.-V. V., Marshall, L., Born, J., Martinetz, T., and Claussen, J. C. (2016). A thalamocortical neural mass model of the EEG during NREM sleep and its response to auditory stimulation. *PLoS Computational Biology*, 12(9):e1005022.

Seibt, J., Richard, C. J., Sigl-Glöckner, J., Takahashi, N., Kaplan, D. I., Doron, G., de Limoges, D., Bocklisch, C., and Larkum, M. E. (2017). Cortical dendritic activity correlates with spindle-rich oscillations during sleep in rodents. *Nature Communications*, 8(1):684.

Sejnowski, T. J. and Destexhe, A. (2000). Why do we sleep? *Brain research*, 886(1-2):208–223.

Silvestri, A. J. and Kapp, B. S. (1998). Amygdaloid modulation of mesopontine peribrachial neuronal activity: implications for arousal. *Behavioral Neuroscience*, 112(3):571–588.

Soma, S., Shimegi, S., Osaki, H., and Sato, H. (2012). Cholinergic modulation of response gain in the primary visual cortex of the macaque. *Journal of Neurophysiology*, 107(1):283–291.

Steriade, M. and Llinás, R. R. (1988). The functional states of the thalamus and the associated neuronal interplay. *Physiological Reviews*, 68(3):649–742.

Steriade, M., McCormick, D. A., and Sejnowski, T. J. (1993a). Thalamocortical oscillations in the sleeping and aroused brain. *Science*, 262(5134):679–685.

Steriade, M., Nuñez, A., and Amzica, F. (1993b). Intracellular analysis of relations between the slow (<1 hz) neocortical oscillation and other sleep rhythms of the electroencephalogram. *The Journal of Neuroscience*, 13(8):3266–3283.

Steriade, M., Paré, D., Bouhassira, D., Deschênes, M., and Oakson, G. (1989). Phasic activation of lateral geniculate and perigeniculate thalamic neurons during sleep with ponto-geniculo-occipital waves. *The Journal of Neuroscience*, 9(7):2215–2229.

Steriade, M., Paré, D., Datta, S., Oakson, G., and Curró Dossi, R. (1990). Different cellular types in mesopontine cholinergic nuclei related to ponto-geniculo-occipital waves. *The Journal of Neuroscience*, 10(8):2560–2579.

Steriade, M., Timofeev, I., and Grenier, F. (2001). Natural waking and sleep states: a view from inside neocortical neurons. *Journal of Neurophysiology*, 85(5):1969–1985.

Sun, Y.-G., Pita-Almenar, J. D., Wu, C.-S., Renger, J. J., Uebele, V. N., Lu, H.-C., and Beierlein, M. (2013). Biphasic cholinergic synaptic transmission controls action potential activity in thalamic reticular nucleus neurons. *The Journal of Neuroscience*, 33(5):2048–2059.

Tononi, G. and Cirelli, C. (2003). Sleep and synaptic homeostasis: a hypothesis. *Brain research bulletin*, 62(2):143–150.

Tononi, G. and Cirelli, C. (2014). Sleep and the price of plasticity: from synaptic and cellular homeostasis to memory consolidation and integration. *Neuron*, 81(1):12–34.

Tononi, G. and Cirelli, C. (2020). Sleep and synaptic down-selection. *The European Journal of Neuroscience*, 51(1):413–421.

Varela, C. (2014). Thalamic neuromodulation and its implications for executive networks. *Frontiers in Neural Circuits*, 8:69.

Varela, C. and Sherman, S. M. (2007). Differences in response to muscarinic activation between first and higher order thalamic relays. *Journal of Neurophysiology*, 98(6):3538–3547.

Watson, B. O., Levenstein, D., Greene, J. P., Gelinas, J. N., and Buzsáki, G. (2016). Network homeostasis and state dynamics of neocortical sleep. *Neuron*, 90(4):839–852.

Williams, J. A. and Reiner, P. B. (1993). Noradrenaline hyperpolarizes identified rat mesopontine cholinergic neurons in vitro. *The Journal of Neuroscience*, 13(9):3878–3883.

Wilson, H. R. and Cowan, J. D. (1972). Excitatory and inhibitory interactions in localized populations of model neurons. *Biophysical Journal*, 12(1):1–24.

Wilson, H. R. and Cowan, J. D. (1973). A mathematical theory of the functional dynamics of cortical and thalamic nervous tissue. *Kybernetik*, 13(2):55–80.

Wilson, M. T., Fulcher, B. D., Fung, P. K., Robinson, P. A., Fornito, A., and Rogasch, N. C. (2018). Biophysical modeling of neural plasticity induced by transcranial magnetic stimulation. *Clinical Neurophysiology*, 129(6):1230–1241.

Wilson, M. T., Goodwin, D. P., Brownjohn, P. W., Shemmell, J., and Reynolds, J. N. J. (2014). Numerical modelling of plasticity induced by transcranial magnetic stimulation. *Journal of Computational Neuroscience*, 36(3):499–514.

Yang, G., Lai, C. S. W., Cichon, J., Ma, L., Li, W., and Gan, W.-B. (2014). Sleep promotes branch-specific formation of dendritic spines after learning. *Science*, 344(6188):1173–1178.

Zhou, Y., Lai, C. S. W., Bai, Y., Li, W., Zhao, R., Yang, G., Frank, M. G., and Gan, W.-B. (2020). REM sleep promotes experience-dependent dendritic spine elimination in the mouse cortex. *Nature Communications*, 11(1):4819.

Zhu, J. J., Lytton, W. W., Xue, J. T., and Uhlrich, D. J. (1999). An intrinsic oscillation in interneurons of the rat lateral geniculate nucleus. *Journal of Neurophysiology*, 81(2):702–711.

Zhu, J. J. and Uhlrich, D. J. (1998). Cellular mechanisms underlying two muscarinic receptor-mediated depolarizing responses in relay cells of the rat lateral geniculate nucleus. *Neuroscience*, 87(4):767–781.